



# Obrabotka metallov - Metal Working and Material Science

Journal homepage: [http://journals.nstu.ru/obrabotka\\_metallov](http://journals.nstu.ru/obrabotka_metallov)



## Study of the stress-strain and temperature fields in cutting tools using laser interferometry

Igor Efimovich <sup>a,\*</sup>, Ivan Zolotukhin <sup>b</sup>

Tyumen Industrial University, 38 Volodarskogo, Tyumen, 625000, Russian Federation

<sup>a</sup>  <https://orcid.org/0000-0002-9060-4988>,  [egor\\_kosin@mail.ru](mailto:egor_kosin@mail.ru), <sup>b</sup>  <https://orcid.org/0000-0002-1517-9117>,  [zolotuhinis@tyuiu.ru](mailto:zolotuhinis@tyuiu.ru)

### ARTICLE INFO

#### Article history:

Received: 13 September 2021

Revised: 28 September 2021

Accepted: 09 November 2021

Available online: 15 December 2021

#### Keywords:

Metal cutting  
 Metal cutting tool  
 Strain measurement  
 Laser interferometry  
 High-speed video recording  
 Stress-strain state  
 Stress distribution  
 Temperature distribution  
 Temperature field  
 Boundary condition  
 Numerical analysis

### ABSTRACT

**Introduction.** The efficiency of the metalworking processes highly depends on the performance of the implemented cutting tools that can be increased by studying its stress-strain state and temperature fields. Existing stress analysis methods either have a low accuracy or are inapplicable for research during the operation of the tools made of materials with high mechanical properties. In addition, the study of temperature fields using known methods is difficult due to the small size of the cutting zone, high temperatures, and a heavy temperature gradient appearing during metal cutting. **The purpose** of this study is to develop new experimental methods for measuring the stress-strain and temperature fields in the cutting tool during its operation using laser interferometry. **The methods** include: obtaining interference fringe patterns using an interferometer with the original design, obtaining the tool deformation field during the cutting process by recording the changes in interference fringe patterns using a high-speed camera, processing fringe patterns with the separation of deformations caused by heating and cutting forces, and calculating temperature fields and stress distributions using mechanical properties and the coefficient of thermal expansion of the tool material. The advantages of the developed methods include: applicability under real operating conditions of the cutting tool, ability to study the non-stationary stress-strain state and temperatures during an operation, and achievement of a high spatial resolution and a small field of view for the investigated surface. **Results and Discussion.** The experimental study confirmed the efficiency of the methods. The results of the study included the fields of stresses and temperatures obtained during the orthogonal cutting of heat-resistant steel with a tool made of cemented tungsten carbide *WC-8Co*. The developed methods can be used to study the cutting tool efficiency at close to real conditions and in obtaining boundary conditions for the study stress-strain state of a workpiece material near the cutting zone.

**For citation:** Efimovich I.A., Zolotukhin I.S. Study of the stress-strain and temperature fields in cutting tools using laser interferometry. *Obrabotka metallov (tekhnologiya, oborudovanie, instrumenty) = Metal Working and Material Science*, 2021, vol. 23, no. 4, pp. 79–92. DOI: 10.17212/1994-6309-2021-23.4-79-92. (In Russian).

## Introduction

Cutting tool efficiency largely determines the economic effectiveness of the technology in which the tool is used. Therefore, studying the stress-strain and temperature states of cutting tool in conditions that are as realistic as possible will allow cutting tool efficiency to be improved.

Many methods exist for studying the stress-strain state of solids, but each has features that limit its application to the problem of studying the stress-strain state of cutting tool. For example, using tensometers or strain gauges to study deformation fields is very difficult because of the small dimensions of the zone under investigation in cutting tools and the high operating temperatures involved during their operation. The split tool method [1] enables study the cutting process under real conditions, but the peculiarities of the cutter design [2] distort the obtained results.

#### \* Corresponding author

Efimovich Igor A., Ph.D. (Engineering), Associate Professor  
 Tyumen Industrial University  
 38 Volodarskogo,  
 625000, Tyumen, Russian Federation  
 Tel.: +7 (3452) 50-49-15, e-mail: [egor\\_kosin@mail.ru](mailto:egor_kosin@mail.ru)

The method involving deposition of brittle coatings on the object under study is unsuitable for recording dynamic deformations, has significant measurement errors, and can only be used for qualitative analysis.

The grid method [3] is difficult to be used with high-strength tool materials because it is difficult to determine changes in the grid node distances caused by the limited deformation of these types of materials. The noncontact mirror method evaluates the effect of grid line distortion due to reflection from the deformable body, but has sufficient sensitivity only when measuring bending deformations. The moiré fringes method is labor-intensive because obtaining and using gratings is a complex process. Digital image correlation [4] makes it possible to automate analysis of the results, but the relatively low sensitivity of this method means that it can only be used for studying deformation of the workpiece material.

The photoelasticity method [5] does not allow experiments with real tool materials, and can be applied only at an extremely low cutting speed when processing workpieces are made of soft materials, owing to the low heat resistance of optically active materials. The photoelastic coating method partially solves these problems, but the peeling of coatings in areas with a high deformation gradient leads to increased measurement errors.

The shadow method (the caustic method) [6] is distinguished by the complexity of decoding the resulting pattern, especially in the case of a complex stress state.

The holographic interferometry method [7] is highly sensitive and can be applied to objects with complex shapes. When using double exposure, the measurement accuracy is high, but continuous dynamic processes cannot be recorded. When implementing the real-time method, it is necessary to isolate the study object from external vibrations.

The method of electronic speckle pattern interferometry [8] makes it possible to measure deformations not only in the direction normal to the surface of the study object, but also along its plane [9]. However, at the same time, the resolution and minimum dimensions of the investigated surface are significantly limited.

The laser interferometry method makes it possible to register strain and stress fields with a high gradient, not only on transparent models, but also on real objects. The disadvantages of this method are the complexity of registering rapidly changing interference patterns while studying dynamic processes and the problems related to their interpretation. The general advantages of optical methods are that they are contactless, highly sensitive, and inertia-free measurement processes.

In studying tool temperature states, contact methods using various types of thermocouples are the most widely used. However, it is difficult to measure temperatures near the tool-chip contact zone using embedded artificial thermocouples. Cut or running thermocouples [10] can only be used to determine the nature of the temperature distribution on the tool faces at low cutting speeds. The semi-artificial thermocouple method is time-consuming, and the use of a split tool distorts the temperature field [11]. The natural (tool-work) thermocouple is applicable only to conductive materials. It allows only the average value of the temperature in the cutting zone to be determined, requires initial calibration, and has low accuracy. Using film microtransducers that are based on resistance thermometers [12] does not solve the problem of obtaining a temperature field due to the difficulty of positioning a large number of sensors on the cutting tool.

Methods that assess the appearance of oxide layers in the air (tempering colors) and irreversible structural changes in the material, including microhardness, make it possible to record only the maximum temperature that appears during the experiment. In addition, changes in the microstructure of heated tool materials, such as cemented tungsten carbide, are insignificant. Thermosensitive coating methods (*PVD* films [10] and thermal paints [13]) have high inertness and low accuracy in measuring temperature fields due to differences in the thermophysical characteristics of the coating material and the study object material, and the processes of heat transfer between them.

The accuracy of infrared thermometry (thermography) methods depends primarily on the accuracy of the experimentally determined emissivity coefficient of the study surface, which can be affected by increasing temperature, surface roughness, and degree of oxidation [14]. The problem of determining and taking into account the change in the emissivity coefficient during heating can be partially solved by using two-color thermometry [15]; however, the influence of surface quality and the degree of oxidation on measurement accuracy remains unaffected. Because the study surface interferes with the oxide films, a false

drift occurs in the measured temperature. The infrared camera has a relatively low spatial resolution because of the long wavelength of thermal radiation, which makes it difficult to study small objects. There are also difficulties in measuring temperatures that vary over a wide range. The high cost of infrared detector arrays and infrared optics limits the application of this method.

The interferometric method of registering temperature deformations of the study object [16] has low inertness, high spatial resolution, and limits the study surface to a small area. Moreover, the coefficient of thermal expansion (*CTE*) required to convert deformations into temperature can be measured with high accuracy using modern dilatometers [17] and does not depend on the extent of surface roughness. The disadvantage of this method is the problem of separating force- and temperature-induced deformations during their combined action, and the limitations associated with the shape of the study object surface.

### *Formulation of the research problem*

At present, analytical [18, 19] and numerical [20] methods are widely used to determine the stress-strain and temperature fields in tools. These methods use idealized distributions of force and thermal loads on the tool faces [21, 22], which are usually obtained analytically, and the processes in the contact zone are greatly simplified. Increased reliability of the analytical results can be achieved by studying experimentally obtained boundary conditions.

The above-mentioned experimental methods of studying the stress-strain state and temperatures have significant disadvantages that limit their applicability and the accuracy of the obtained results. Therefore, the development of new experimental methods for studying the phenomena that occur during the operation of various types of tools is a significant scientific goal.

## Methods

New experimental methods for studying deformations [23] and temperature fields [24] in cutting tools are developed to overcome the limitations of current experimental methods and to make experimental conditions more realistic. We also created a laser interferometric rig [25] to implement these methods.

The principal scheme of the experimental setup is illustrated in Fig. 1. The processed material was formed as a disc (1) and was fixed on a rotating mandrel (2). The study tool (3), installed in the tool holder (4), moves together with the optical part of the rig in the radial direction at the feed rate  $S$ . To obtain an interference pattern, an interferometer formed by the polished tool surface (5) and fixed on the tool holder optical wedge (6) was used. The light source was a laser (7), and a beam expander (8) was applied to increase the beam aperture. The initial polarization of the laser beam is horizontal, which allows the beam to pass through a polarized beam splitter (9) without loss. After passing through the quarter-wave plate (10), the beam changes to circular polarization with counterclockwise rotation. In the interferometer, the beam is divided into measurement and reference beams. The reference beam is formed by the part of the original beam that reflects from the optical wedge surface facing the tool. The part of the original beam that passes through the optical wedge forms a measurement beam that strikes the polished surface of the tool. After reflection of both beams, their polarization vectors rotate clockwise, and when they meet again in the optical wedge, they interfere. Because of the change in the vector rotation direction, after passing through the wave plate, the resulting beam becomes vertically polarized and is reflected from the diagonal beam splitter surface toward the

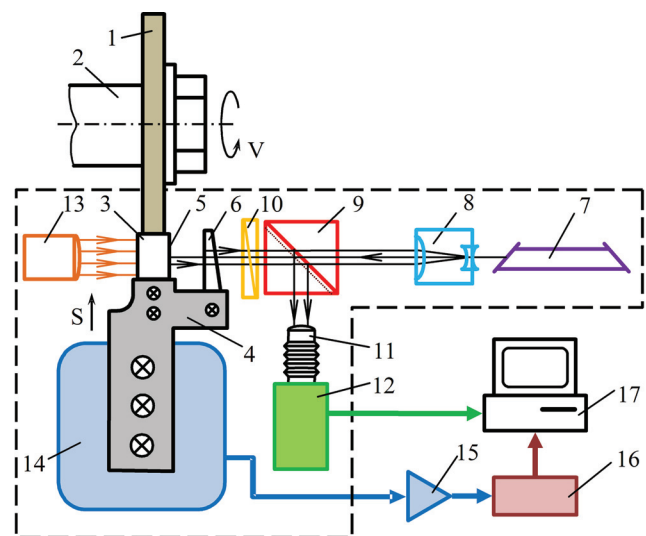


Fig. 1. Schematic diagram of the experimental rig

lens (11) of the camera (12). A collimated backlight was used (13) to determine the tool and workpiece contours. A strain gauge multicomponent dynamometer (14) with an amplifier (15) and an analog-to-digital converter (16) were used to record the force components during the cutting process. Interference fringes and the acting cutting forces were recorded in the computer memory (17).

The use of a polarized beam splitter cube and a quarter-wave plate made it possible to minimize the ghost reflections of the laser beam, which practically eliminated the moiré effect and significantly reduced the

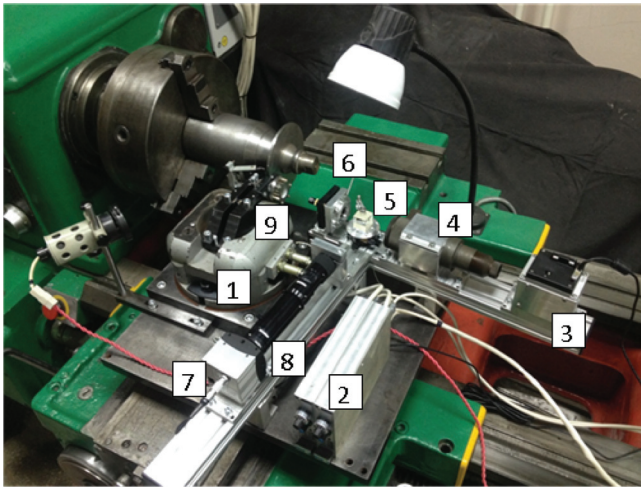


Fig. 2. View of the experimental rig based on a lathe

loss of luminous flux. It improved the image quality of the recorded interference patterns, which is necessary for high-speed recording with brief exposure.

The experimental setup was mounted on a retrofitted lathe model 163 (Fig. 2). A thyristor drive *KEMTOK* with a *DC* motor was used to rotate the spindle, which provided a stepless adjustment of the cutting speed. On the cross slide of the machine, the *UDM-600* dynamometer (1) with a tool holder, two single-channel *RDP 628* strain gauge amplifiers (2), and two aluminum profile rails were fixed on a base plate. A single-mode single-frequency *DPSS* laser *LCM-S-III* (3) with a wavelength of 532 nm, a beam expander (4), adjustable holders with a beam splitter (5), and a zero-order wave plate (6) were installed on one guide. A high-speed digital video camera *Fastec HiSpec 2-HR* (7) with a *NAVITAR Zoom 6000* lens (8) was fixed on the second rail. The optical wedge (9) was mounted on a tool holder in an adjustable frame. All optical elements had antireflective coatings, and the tool holder design was optimized to improve the dynamic characteristics of the dynamometer. In the current version, the developed methods are applicable only for dry cutting without the use of cutting fluids.

The interference patterns obtained during the experiment include information about changes in  $\Delta t_c$  of the cutting tool width  $t_c$ :

$$\Delta t_c = \frac{1}{n} m \lambda, \quad (1)$$

where  $n$  is the refractive index of air ( $n = 1$  can be taken with sufficient accuracy),  $m$  is the number of interference fringes that have moved relative to the point of interest (the interference fringe order), and  $\lambda$  is the wavelength (for the used laser  $\lambda = 532$  nm).

At the same time, the lateral strains can be found as follows:

$$\varepsilon_z = \frac{\Delta t_c}{t_c}. \quad (2)$$

Substituting (2) into (1), we obtain:

$$\varepsilon_z = \frac{m \lambda}{t_c}. \quad (3)$$

To determine the difference in the interference fringe orders  $m$ , two interference patterns need to be analyzed – the pattern before the application of load and after loading; using these patterns in the section of interest (for example, along the tool faces of the cutting tool), the fringe order distributions ( $m_1$  and  $m_2$ , respectively) can be found. By subtracting the obtained plots, the total deformation (thermal and forces acting) plot  $m_s = (m_2 - m_1)$  was obtained. To obtain a plot of only deformations by forces acting on  $m_p$ , the plot of thermal deformations  $m_t$  is subtracted from the  $m_s$  plot:  $m_p = m_s - m_t$ . The plot of thermal deformations  $m_t$  can be obtained from the interference pattern recorded immediately after the rapid interruption of the cutting process.

According to *Hooke's Law*,

$$\varepsilon_z = -\frac{\mu}{E}(\sigma_x + \sigma_y), \quad (4)$$

where  $\mu$  is the Poisson ratio, and  $E$  is the *Young's modulus*, and  $\sigma_x$  and  $\sigma_y$  are the normal stresses along the  $X$ - and  $Y$ -axis directions, respectively.

Using equation (1) for the case when there is only force action ( $m = m_p$ ) with equations (2) and (4), and considering  $(\sigma_x + \sigma_y) = \Theta$ , we can obtain an equation for calculating the sum of the normal stresses  $\Theta$  as:

$$\Theta = -\frac{E \Delta t_c}{\mu t_c} = -\frac{E m_p \lambda}{\mu t_c}. \quad (5)$$

In this way, the interference pattern analysis allows us to determine the fringe order differences at the point of interest in the cutting part of the tool, and using this information, determine the sums  $\Theta$  of the stress components at this point.

Before calculating the stress components, the field of the sums  $\Theta$  obtained from the experiment should be harmonized. The harmonization of the sums field  $\Theta$  is performed by solving the differential equation of equilibrium:

$$\frac{\partial^2 \Theta}{\partial x^2} + \frac{\partial^2 \Theta}{\partial y^2} = 0. \quad (6)$$

Equation (6), in finite difference form for a square grid (Fig. 3, *a*), has the following form:

$$\Theta_{J+1,N} + \Theta_{J,N+1} + \Theta_{J-1,N} + \Theta_{J,N-1} - 4 \cdot \Theta_{J,N} = 0, \quad (7)$$

and for harmonization purposes, it can be transformed into:

$$\Theta_{J,N} = \frac{1}{4}(\Theta_{J-1,N} + \Theta_{J,N+1} + \Theta_{J+1,N} + \Theta_{J,N-1}). \quad (8)$$

After harmonization of the sums  $\Theta$  field by the iteration method to the required accuracy, the components of stresses  $\sigma_x$ ,  $\sigma_y$ , and  $\tau_{xy}$  may be calculated. For the stress calculation, the location of the grid  $x$ -axis along the clearance face of the cutting tool is most convenient when it is formed as a wedge (Fig. 4).

In orthogonal cutting conditions, the tool is in a plane stress state, which must satisfy the equilibrium equations:

$$\frac{\partial \sigma_x}{\partial x} + \frac{\partial \tau_{xy}}{\partial y} + X = 0, \quad (9)$$

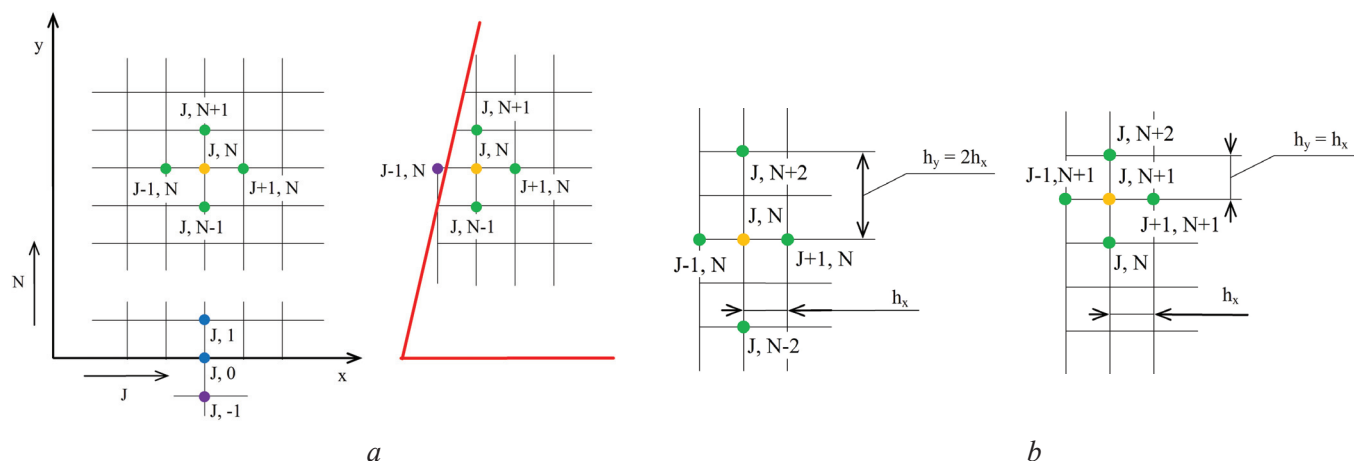


Fig. 3. Scheme to number the nodes of the square grid (*a*) and scheme to end nodes of grid lines (*b*)

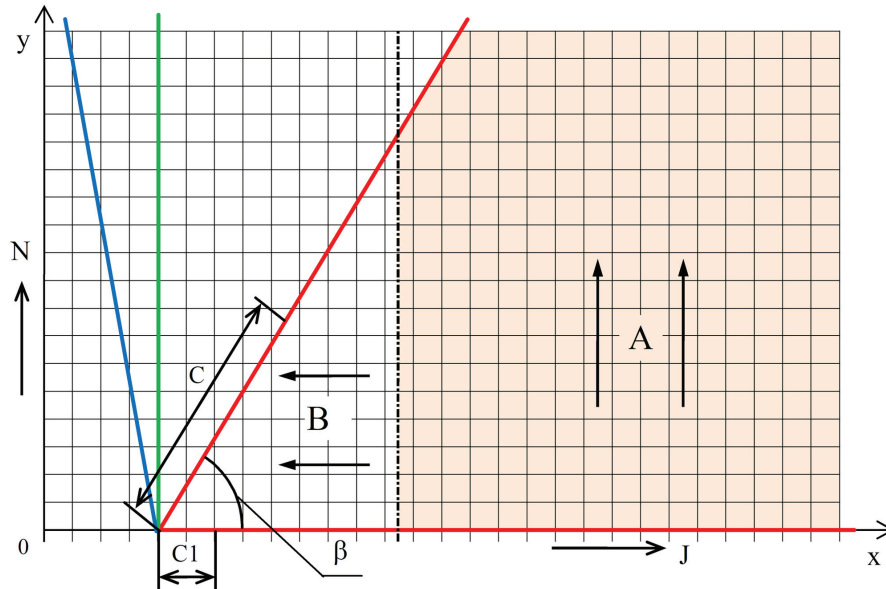


Fig. 4. Scheme to grid orientation relative to the cutting tool:

$C$  – length of the tool in contact with the chip;  $C1$  – length of the tool in contact with the workpiece;  $\beta$  – lip angle

$$\frac{\partial y_x}{\partial x} + \frac{\partial \Phi_{xy}}{\partial y} + Y = 0, \quad (10)$$

where  $X$  and  $Y$  are the components of the internal forces acting on the solid (tool). Because only external forces act on the tool, the internal forces are constant or zero; that is, they can be taken as  $X = Y = 0$ . Taking this into account, and differentiating equation (9) with respect to  $x$  and equation (10) with respect to  $y$ , we obtain:

$$\frac{\partial^2 \sigma_y}{\partial x^2} + \frac{\partial^2 \tau_{xy}}{\partial x \partial y} = 0, \quad (11)$$

$$\frac{\partial^2 \sigma_y}{\partial y^2} + \frac{\partial^2 \tau_{xy}}{\partial x \partial y} = 0. \quad (12)$$

Subtracting equations (11) and (12) we obtain:

$$\frac{\partial^2 \sigma_y}{\partial y^2} + \frac{\partial^2 \sigma_x}{\partial x^2} = 0. \quad (13)$$

Transforming the last equation by making the substitution  $\sigma_x = (\Theta - \sigma_y)$ , we obtain

$$\frac{\partial^2 \sigma_y}{\partial x^2} + \frac{\partial^2 \sigma_y}{\partial y^2} = \frac{\partial^2 \Theta}{\partial x^2}. \quad (14)$$

If equation (14) is represented in finite difference form (the node positions illustrated in Fig. 3, a), we obtain

$$\sigma_{yJ+1,N} + \sigma_{yJ,N+1} + \sigma_{yJ-1,N} + \sigma_{yJ,N-1} - 4\sigma_{yJ,N} = \Theta_{J+1,N} - 2\Theta_{J,N} + \Theta_{J-1,N}. \quad (15)$$

For extrapolation (during line-by-line separation of the stress sums), the obtained equation (15) should be transformed with respect to members  $\sigma_{yJ,N+1}$ ,  $\sigma_{yJ+1,N}$ ,  $\sigma_{yJ-1,N}$  and  $\sigma_{yJ,N-1}$ ; for harmonization equation should be transformed with respect to member  $\sigma_{yJ,N}$ . In zone  $A$ , the calculation is performed from the

boundary into the tool body (see Fig. 4), and to calculate  $\sigma_{yJ,N+1}$ , equation (15) is used for lines with  $N = 2$  or more.

To calculate  $\sigma_{yJ,1}$  in the line  $N = 1$ , equations (10) and (15) should be rearranged in finite difference form for point  $(J, 0)$ . After their transformation, considering that the values of  $\sigma_y$  and  $\tau_{xy}$  on the boundary outside the contact zone are equal to zero, we obtain the equation:

$$\sigma_{yJ,1} = \frac{1}{2}(\Theta_{J+1,0} - 2\Theta_{J,0} + \Theta_{J-1,0}). \quad (16)$$

To find the values of  $\sigma_y$  at the edges of the grid lines, equation (15) should be rearranged in finite difference form using a doubled step along the  $y$ -axis, that is, replacing  $h_y = 2 \times h_x$  (Fig. 3b on the left), and solved with respect to member  $\sigma_{yJ,N+2}$ :

$$\sigma_{yJ,N+2} = 4 \cdot (\Theta_{J+1,N} - 2 \cdot \Theta_{J,N} + \Theta_{J-1,N}) + 10 \cdot \sigma_{yJ,N} - 4 \cdot (\sigma_{yJ+1,N} + \sigma_{yJ-1,N}) - \sigma_{yJ,N-2}. \quad (17)$$

After determining  $\sigma_{yJ,N+2}$ , we can find  $\sigma_{yJ-1,N+1}$  and  $\sigma_{yJ+1,N+1}$  at the edges of grid line  $N+1$  (Fig. 3, *b* on the right), by transforming equation (15) with respect to the center node  $(J, N+1)$ .

For zone *B* (see Fig. 4), the calculation was performed in the same manner, by taking into account the change in direction, that is, instead of layers  $N$  of zone *A*, layers  $J$  were considered.

The normal stress  $\sigma_x$  at each node is determined by the equation:

$$\sigma_x = \Theta - \sigma_y. \quad (18)$$

The tangential stress component  $\tau_{xy}$  can be determined from the equilibrium equations (11) and (12), if they are transformed into a finite difference form:

$$\tau_{xyJ,N+1} = \tau_{xyJ,N-1} + \tau_{xJ+1,N} - \tau_{xJ-1,N} \quad (19)$$

and in zone *B*:

$$\tau_{xyJ-1,N} = \tau_{xyJ+1,N} - \tau_{yJ,N+1} + \tau_{yJ,N-1}. \quad (20)$$

For the first grid line of zone *A*, the equation becomes:

$$\tau_{xyJ,1} = \frac{\sigma_{xJ+1,0} - \sigma_{xJ-1,0}}{2}. \quad (21)$$

In this way, using equations (15) to (21), it is possible to separate the stress sums  $\Theta$  obtained as a result of the interference pattern analysis; that is, we can calculate the stress components  $\sigma_x$ ,  $\sigma_y$  and  $\tau_{xy}$ .

To calculate the temperature field, the plot  $m_1$  obtained before the application of the load (i.e., for a cold tool), is subtracted from the fringe order plot  $m_3$  obtained immediately after the interruption of the cutting process. Thus, a plot of the fringe order  $m_t = (m_3 - m_1)$  can be obtained for the section of interest of the heated tool.

If there are temperature deformations, taking into account temperature stresses and formula (3), Hooke's law for a plane stress state can be represented as:

$$\varepsilon_z = \frac{m_t \lambda}{t_u} = -\frac{\mu}{E}(\sigma_x + \sigma_y) + \alpha(T_t - T_0), \quad (22)$$

where  $(T_t - T_0)$  is the temperature change from the initial temperature  $T_0$  to the reached temperature  $T_t$  at the moment of interest during tool operation,  $(\sigma_x + \sigma_y)$  is the sum of thermal stresses, and  $\alpha$  is the CTE of the tool material [26].

Thermal stresses, according to various research results, are usually less than 40 % of the stresses caused by cutting forces during tool operation. If we take  $(\sigma_x + \sigma_y) = 0$ , then during rough turning of steel (e.g., at  $T_t = 740$  K for cemented tungsten carbide *WC-8Co* [grade *VK8*]) with  $\alpha = 4.7 \times 10^{-6} \text{ K}^{-1}$ ,  $E = 596$  GPa,

$\mu = 0.32$  and with the maximum value of the stresses sum  $\Theta = 1600$  MPa in the cutting wedge), the component of deformations caused by thermal stresses will not exceed 14 % of the total tool deformation in the zone with maximum temperature gradient. Therefore, the temperatures at the grid nodes can be determined with sufficient accuracy in engineering calculations by using the formula obtained from equation (22) as:

$$T_t = \frac{m_t \lambda}{t_n \alpha} + T_0. \quad (23)$$

The proposed methods were implemented in programs created using *MATLAB* to calculate the stress components and temperatures.

## Results and Discussion

To study the efficiency of the methods, an experiment was performed in which steel grade *X13Cr11Ni-2W2MoV (EI961)* was turned using a tool made of cemented tungsten carbide grade *WC-8Co (VK8)*, with a clearance angle  $\gamma = 10^\circ$ , rake angle  $\alpha = -5^\circ$ , cutting speed  $V = 0.1$  m/s, and feed  $S = 0.15 \times 10^{-3}$  m/rev. Interference patterns obtained by video recording with a frame rate of  $16 \times 10^3$  fps under the cutting conditions mentioned above, are shown in Fig. 5.

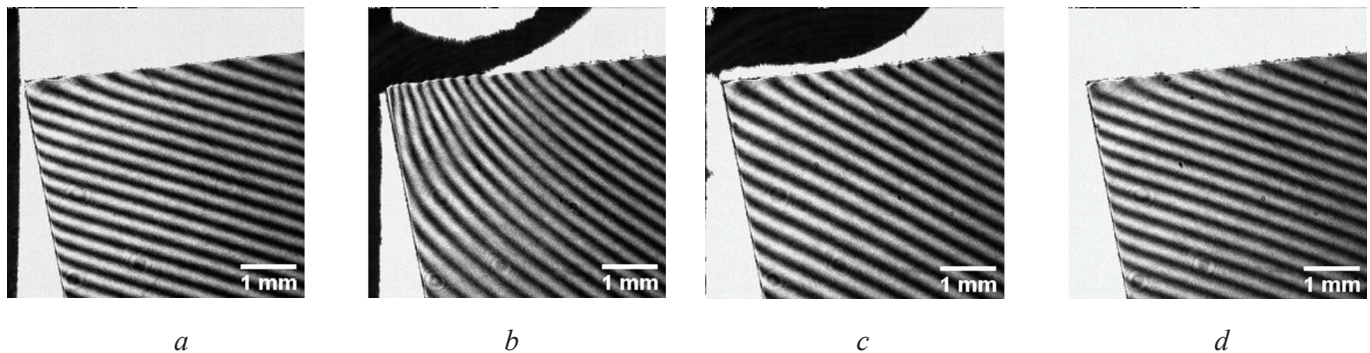


Fig. 5. Interference fringe patterns (camera frame rate  $16 \cdot 10^3$  fps):

*a* – before the cutting process; *b* – during the cutting process (maximum load); *c* – immediately after the interruption of the process; *d* – one second after the interruption of the process

Figure 6 shows diagrams of the fringe order  $m$  distributions along the rake and clearance faces of the tool (with respect to distance  $R$  from the cutting edge).

Figure 7 shows the fields of stress components  $\sigma_x$ ,  $\sigma_y$ , and  $\tau_{xy}$  and the temperature field obtained using the developed methods.

The analysis of the stress component  $\sigma_x$  distributions shows that the main stresses are compression stresses and their maximum values are observed on the rake face near the cutting edge. The change in component  $\sigma_y$  along the rake face is extreme, with a minimum observed in the tool-chip contact zone. As we move closer to the cutting edge, the stress component  $\sigma_y$  increases and changes sign. The change in the tangential component  $\tau_{xy}$  on the rake face is also extreme. As we move closer to the cutting edge, the  $\tau_{xy}$  component first decreases to a minimum negative value, and then increases and changes sign. In the contact zone, a narrow zone of negative  $\tau_{xy}$  values is observed on the clearance face, and outside the contact zone, the component  $\tau_{xy} = 0$ .

The temperature field was quite uniform. The temperature values were relatively low because of the high thermal conductivity of the tool material and low cutting speed. The maximum temperature was observed at the cutting edge. Moving away from the edge, the temperature decreased, while a larger gradient was observed along the rake face.

The nature of the temperatures and stress distributions obtained by proving the efficiency of the developed methods coincide with the results obtained by alternative methods in other studies [1, 14].

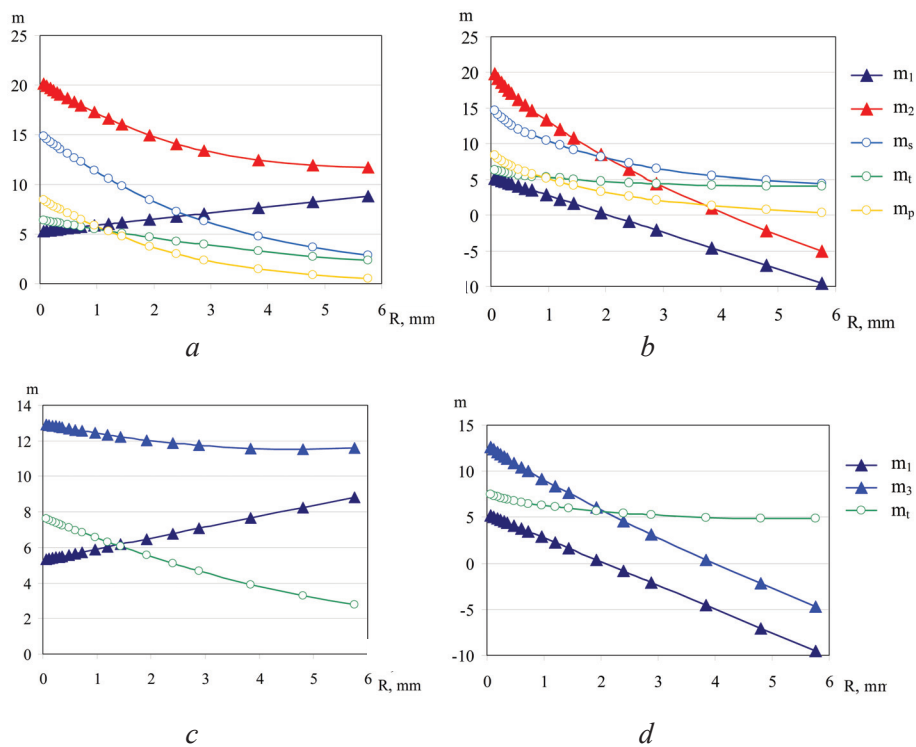


Fig. 6. Fringe order distributions during the cutting process for the rake (a) and clearance (b) faces; immediately after the interruption of the process for the rake (c) and clearance (d) faces

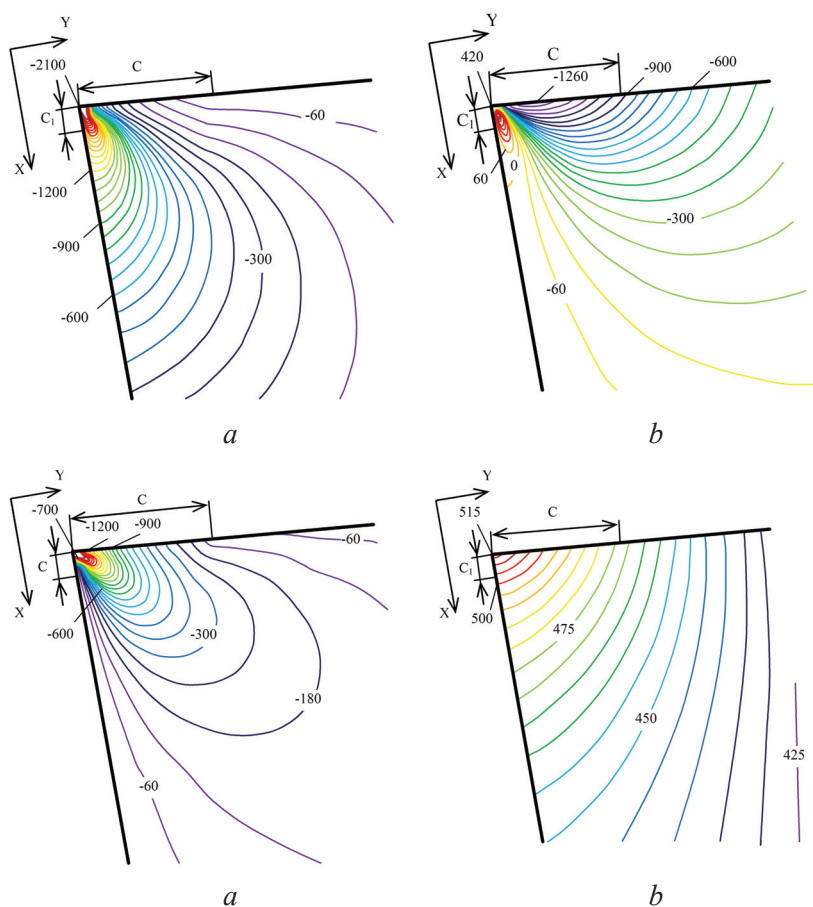


Fig. 7. Distribution of stress components  $\sigma_x$  (a),  $\sigma_y$  (b), and  $\tau_{xy}$  (c) in MPa and the temperature field (d) in K

## Conclusion

New experimental methods for studying deformation and temperature fields based on laser interferometry are developed. These methods make it possible to perform experiments with real workpiece and tool materials under real dynamic cutting-process conditions.

In contrast to infrared thermometry, our method for studying temperature fields has high spatial resolution and a significantly smaller field of view, owing to the use of light in the visible range of the spectrum. In addition, the method is more reliable because there is no interference from short-wave radiation on oxide films and because the coefficient of thermal expansion is used for calculating temperatures, which, unlike emissivity, does not depend on the surface quality and can be measured with high accuracy on modern dilatometers.

The special design of the interferometer, including an optical wedge rigidly fixed to the tool holder, made it possible to minimize the influence of vibrations, which is the main error source in methods based on interferometry. In addition, the use of polarized optical components reduced the loss of luminous flux and significantly increased the quality of the recorded interference patterns, which is very important for high-speed video recording with ultra-fast exposure.

The efficiency of the developed interferometric methods is experimentally confirmed by cutting high-alloy steel grade *X13Cr11Ni2W2MoV (EI961)* with a tool made of cemented tungsten carbide grade *WC-8Co (VK8)* with a negative rake angle of  $5^\circ$ ; stress components and temperature fields in the tool are obtained.

## References

1. Buryta D., Sowerby R., Yellowley I. Stress distributions on the rake face during orthogonal machining. *International Journal of Machine Tools and Manufacture*, 1994, vol. 34, iss. 5, pp. 721–739. DOI: 10.1016/0890-6955(94)90054-X.
2. Laakso S.V.A., Bushlya V., Ståhl J.-E. The correct way of splitting tools – Optimization of instrument design for measuring contact stress distribution. *Procedia Manufacturing*, 2018, vol. 25, pp. 97–102. DOI: 10.1016/j.promfg.2018.06.062.
3. Grédiac M., Sur F., Blaysat B. The grid method for in-plane displacement and strain measurement: a review and analysis. *Strain*, 2016, vol. 52, iss. 3, pp. 205–243. DOI: 10.1111/str.12182.
4. Dong Z., Zhang X.-M., Xu W.-J., Ding H. Stress field analysis in orthogonal cutting process using digital image correlation technique. *Journal of Manufacturing Science and Engineering*, 2017, vol. 139, p. 031001. DOI: 10.1115/1.4033928.
5. Ramesh K., Sasikumar S. Digital photoelasticity: recent developments and diverse applications. *Optics and Lasers in Engineering*, 2020, vol. 135. DOI: 10.1016/j.optlaseng.2020.106186.
6. Isogimi K., Kitagawa T., Kurita H. Fundamental research of stress analysis in cutting tool by means of caustics method. *Journal of the Japan Society for Precision Engineering*, 1988, vol. 54, iss. 2, pp. 390–395. DOI: 10.2493/jjspe.54.390.
7. Flores-Moreno J.M., Torre-Ibarra M.D.L., Hernandez-Montes M.D.S., Santoyo F.M. DHI contemporary methodologies: a review and frontiers. *Optics and Lasers in Engineering*, 2020, vol. 135, p. 106184. DOI: 10.1016/j.optlaseng.2020.106184.
8. Torre I.M. De la, Hernandez-Montes M.D.S., Flores-Moreno J.M., Santoyo F.M. Laser speckle based digital optical methods in structural mechanics: a review. *Optics and Lasers in Engineering*, 2016, vol. 87, pp. 32–58. DOI: 10.1016/j.optlaseng.2016.02.008.
9. Razumovsky I.A. *Interferentsionno-opticheskie metody mekhaniki deformiruemogo tverdogo tela* [Interference-optical methods of solid mechanics]. Moscow, Bauman MSTU Publ., 2007. 240 p. ISBN 5-7038-2731-4.
10. Longbottom J.M., Lanham J.D. Cutting temperature measurement while machining – a review. *Aircraft Engineering and Aerospace Technology*, 2005, vol. 77, iss. 2, pp. 122–130. DOI: 10.1108/00022660510585956.
11. Komanduri R.A., Hou Z.B. Review of the experimental techniques for the measurement of heat and temperatures generated in some manufacturing processes and tribology. *Tribology International*, 2001, vol. 34, pp. 653–682. DOI: 10.1016/S0301-679X(01)00068-8.
12. Yoshioka H., Hashizume H., Shinno H. In-process microsensor for ultraprecision machining. *IEE Proceedings – Science Measurement and Technology*, 2004, vol. 151, no. 2. DOI: 10.1049/ip-smt:20040375.



13. Davies M.A., Ueda T., M'Saoubi R., Mullany B., Cooke A.L. On the measurement of temperature in material removal processes. *CIRP Annals*, 2007, vol. 56, iss. 2, pp. 581–604. DOI: 10.1016/j.cirp.2007.10.009.
14. Pujana J., Campo L. del, Pérez-Sáez R.B., Tello M.J., Gallego I., Arrazola P.J. Radiation thermometry applied to temperature measurement in the cutting process. *Measurement Science and Technology*, 2007, vol. 18, no. 11, pp. 3409–3416. DOI: 10.1088/0957-0233/18/11/022.
15. Hijazi A., Sachidanandan S., Singh R., Madhavan V. A calibrated dual-wavelength infrared thermometry approach with non-greybody compensation for machining temperature measurements. *Measurement Science and Technology*, 2011, vol. 22, no. 2, pp. 1–13. DOI: 10.1088/0957-0233/22/2/025106.
16. Magunov A.N. *Laser thermometry of solids*. Cambridge, Cambridge International Science Publishing, 2006. 240 p. ISBN 978-1-904602-12-5.
17. James J.D., Spittle J.A., Brown S.G.R., Evans R.W. A review of measurement techniques for the thermal expansion coefficient of metals and alloys at elevated temperatures. *Measurement Science and Technology*, 2001, vol. 12, pp. R1–R15. DOI: 10.1088/0957-0233/12/3/201.
18. Goryainov V.V., Popov M.I., Chernyshov A.D. Solving the stress problem in a sharp wedge-whaped cutting tool using the quick decomposition method and the problem of matching boundary conditions. *Mechanics of Solids*, 2019, vol. 54, no. 7, pp. 1083–1097. DOI: 10.3103/S0025654419070094.
19. Klocke F., Brockmann M., Gierlings S., Veselovac D. Analytical model of temperature distribution in metal cutting based on potential theory. *Mechanical Sciences*, 2015, vol. 6, pp. 89–94. DOI: 10.5194/ms-6-89-2015.
20. Arrazola P.J., Özel T., Umbrello D., Davies M., Jawahir I.S. Recent advances in modelling of metal machining processes. *CIRP Annals*, 2013, vol. 62, iss. 2, pp. 695–718. DOI: 10.1016/j.cirp.2013.05.006.
21. Bezyazychnyi V.F., Szczerek M. Thermal processes research development in machine-building technology. *Journal of Mining Institute*, 2018, vol. 232, pp. 395–400. DOI:10.31897/pmi.2018.4.395.
22. Olt J.J., Liyvapuu A.A., Liivapuu O.O., Maksarov V.V., Tärkla T.T. Mathematical modelling of cutting process system. *Engineering Mathematics I*. Cham, Springer, 2016, pp. 173–186. DOI: 10.1007/978-3-319-42082-0\_11.
23. Efimovich I.A., Shvetsova E.I. *Sposob issledovaniya deformatsii rezhushchego instrumenta v protsesse rezaniya* [Method for study of cutting tool deformation in process of cutting]. Patent RF, no. 2436039, 2010.
24. Efimovich I.A., Zolotukhin I.S., Shvetsova E.I. *Sposob opredeleniya temperaturnykh polei v rezhushchei chasti instrumenta v protsesse rezaniya* [Method for determination of temperature fields in the cutting part of the instrument in process of cutting]. Patent RF, no. 2442967, 2010.
25. Efimovich I.A., Zolotukhin I.S., Efimovich V.I. *Interferometricheskaya ustanovka* [Interferometric rig]. Patent RF, no. 151653, 2014.
26. Efimovich I.A., Zolotukhin I.S., Zav'yalov E.S. Temperaturnyi koeffitsient lineinogo rasshireniya vol'framo-kobal'tovykh tverdykh splavov [Thermal coefficient of linear expansion of tungsten-cobalt cemented carbide]. *Obrabotka metallov (tekhnologiya, oborudovanie, instrumenty) = Metal Working and Material Science*, 2019, vol. 21, no. 3, pp. 129–140. DOI: 10.17212/1994-6309-2019-21.3-129-140.

## Conflicts of Interest

The authors declare no conflict of interest.

© 2021 The Authors. Published by Novosibirsk State Technical University. This is an open access article under the CC BY license (<http://creativecommons.org/licenses/by/4.0/>).

